

The nearby eclipsing stellar system δ Velorum

II. First reliable orbit for the eclipsing pair

T. Pribulla^{1,2}, A. Merand³, P. Kervella⁴, M. Vaňko², I.R. Stevens⁵, R. Chini^{6,7}, V. Hoffmeister⁶, O. Stahl⁸, A. Berndt¹,
M. Mugrauer¹, and M. Ammler-von Eiff⁹

¹ Astrophysikalisches Institut und Universitäts-Sternwarte, Schillergäßchen 2-3, 07745 Jena, Germany
e-mail: [alex,markus]@astro.uni-jena.de

² Astronomical Institute, Slovak Academy of Sciences, 059 60 Tatranská Lomnica, Slovakia
e-mail: [pribulla,vanko]@ta3.sk

³ European Southern Observatory, Alonso de Cordova 3107, Vitacura, Santiago, Chile
e-mail: amerand@eso.org

⁴ LESIA, Observatoire de Paris, CNRSUMR8109, UPMC, Université Paris Diderot, 5 Place Jules Janssen, 92195 Meudon, France
e-mail: Pierre.Kervella@obspm.fr

⁵ School of Physics and Astronomy, University of Birmingham, Edgbaston, Birmingham, B15 2TT, United Kingdom
e-mail: irs@star.sr.bham.ac.uk

⁶ Astronomisches Institut, Ruhr-Universität Bochum, Universitätsstr. 150, 44801 Bochum, Germany
e-mail: [chini,vhoff]@astro.rub.de

⁷ Facultad de Ciencias, Universidad Católica del Norte, Antofagasta, Chile

⁸ ZAH, Landessternwarte Königstuhl, 69117 Heidelberg, Germany

⁹ Institut für Astrophysik, Georg-August-Universität, Friedrich-Hund-Platz 1, 37077 Göttingen, Germany
e-mail: ammler@mps.mpg.de

Received September 15, 2010; accepted September 16, 2010

ABSTRACT

Context. The nearby multiple system δ Velorum contains a widely detached eclipsing binary and a third component.

Aims. The system offers an opportunity to determine the set of fundamental parameters (masses, luminosities, and radii) of three coeval stars with sufficient precision to test models of stellar evolution.

Methods. Extensive high-resolution spectroscopy is analyzed by the broadening function technique to provide the first spectroscopic orbit for the eclipsing pair. Simultaneous analysis of the spectroscopic data and the SMEI satellite light curve is performed to provide astrophysical parameters for the components. Modified Roche model assuming eccentric orbit and asynchronous rotation is used.

Results. The observations show that components of the eclipsing pair rotate at about 2/3 of the break-up velocity which prevents any chemical peculiarity and results in non-uniform surface brightness. Although the inner orbit is eccentric, no apsidal motion is seen during the SMEI photometric observations. The orbital parameters for the inner orbit are as follows: eccentricity $e = 0.290$, longitude of the periastron passage $\omega = 109^\circ$, inclination 89.0° .

Conclusions. Component's masses $M_{Aa} = 2.53 \pm 0.11 M_\odot$, $M_{Ab} = 2.37 \pm 0.10 M_\odot$ and $M_B \sim 1.5 M_\odot$ combined with inferred radii of Aa and Ab components indicate that the eclipsing pair has already left the Main sequence and the estimated age of the system is about 400 Myr.

1. Introduction

δ Velorum is one of the fifty brightest stars on the sky ($V = 1.96$) and it is located only 24.4 pc from the Sun ($\pi = 40.90 \pm 0.38$ mas; ESA 1997). For a long time it has been known that it is a visual binary composed of the brighter component A with $H_p = 1.99$ and the fainter component B with $H_p = 5.57$ orbiting in a wide 142-year orbit (see Argyle et al., 2002).

Surprisingly, observations by visual observers, supported by photometry from the Galileo star tracker, led to the discovery that the brighter component of the visual pair is an eclipsing binary with $P = 45.15$ days (Otero et al., 2000). No complete and reliable observations of both eclipses exist, however.

Spectroscopic observations of δ Velorum are also very limited. Levato (1972) obtained medium-dispersion (40 Å/mm) photographic spectra of the system and determined an A1V

spectral type and projected rotational speed of $v \sin i = 85$ km s⁻¹. Later, δ Velorum was included into the survey of early-type Hipparcos targets of Royer et al. (2002), who took one échelle spectrum of the system. Fourier transforms of two spectral lines gave $v \sin i = 150$ km s⁻¹, rather inconsistent with the previous result. These measurements very probably included both A and B visual components. No line doubling has been noticed.

The δ Velorum system has been observed interferometrically by Kellerer et al. (2007). Their observations consist of 17 squared visibility measurements using VLTI/VINCI. Although VLTI clearly resolved the eclipsing pair, the presence of the visual component and the small number of observations caused the estimated parameters to be very preliminary and uncertain: semi-major axis $a = 5.7 \pm 0.3 \cdot 10^{10}$ m, radii of the components $R_{Aa} = 6.0 \pm 0.5 R_\odot$, $R_{Ab} = 3.3 \pm 0.6 R_\odot$, eccentricity

$e = 0.230 \pm 0.005$, angle between the major axis and line of sight $\omega' = -(20 \pm 3)^\circ$ ¹, and longitude of the ascending node $\Omega = 27.4 \pm 1.2^\circ$ with a reduced $\chi_r^2 = 2.6$.

Later Gáspár et al. (2008) discovered a spectacular IR bow-shock around δ Velorum at 24 and $70\mu\text{m}$ using Spitzer/MIPS images. This very large structure, $\sim 1'$, was explained by the authors as a result of the heating and compression of the interstellar medium by the photons from δ Velorum as the trio moves through the interstellar medium. Very recently, Kervella et al. (2009) resolved the wide visual pair AB using the VISIR and NACO instruments at the VLT and obtained separate photometry of Aa, Ab and B components. Their photometry did not support the large radii of the components, as found by Kellerer et al. (2007). Mid-infrared observations presented by the authors exclude the presence of a circumstellar thermal excess around the system.

In spite of above results it is clear that the eclipsing pair still waits for a sound light-curve (hereafter LC) and spectroscopic analysis providing reliable orbit and absolute parameters of the components.

2. New Observations

2.1. SMEI satellite photometry

Because of its high brightness δ Velorum is a rather difficult target for ground-based photometry. Unlike for faint stars where the quality of observations is dictated mostly by the shot and read-out noise, observations of the brightest stars suffer from the lack of nearby and sufficiently bright comparisons. Accompanying changes/differences in atmosphere transparency result in large red noise. Covering eclipses of the eclipsing pair from ground-based observations is complicated by the long orbital period of $P = 45.15$ days.

In the case of δ Velorum the Solar Mass Ejection Imager (SMEI) provides a LC of sufficient precision. In addition to its primary task, SMEI, attached to the Coriolis satellite, is capable of producing high-precision photometric time-series for stars up to $V = 7$ (see e.g., Bruntt et al., 2006; Tarrant et al., 2008; Spreckley & Stevens, 2008). Similar to the MOST satellite (see Walker et al., 2003), Coriolis stays close to the dawn-dusk terminator with an orbital frequency of 14.17 cycles/day. Its three cameras take narrow scans of the sky, but when combined, they provide almost full-sky coverage. Of the 3 cameras that make up SMEI, camera 3 operates at a higher temperature and has degraded photometric performance. We do not use data from camera 3 and this means we do not have continuous coverage of δ Velorum. See Goss et al. (2010) and references therein, for more details about SMEI.

The LC of δ Velorum generated from the SMEI images consist of 11195 points covering 5.6 years. The data were obtained during 7 observing seasons (winter half of the year). The photometry is rather sparse, consisting of mostly one observation per orbit. Due to the very long orbital period of the eclipsing pair, and the short duration of the eclipses, ΔT (pri) = 0.613 days and ΔT (sec) = 0.896 days, only about 350 observations were obtained during the eclipses. Combining 9 secondary minima determined from the SMEI photometry and that obtained by the Galileo satellite tracker (Otero, 2000) results in the following ephemeris: Min II = HJD 2447851.693(9) + 45.15023(7) $\times E$. The SMEI LC does not show apsidal motion. Because of the low angular resolution of the SMEI cameras, both components of the visual pair contribute to the extracted LC.

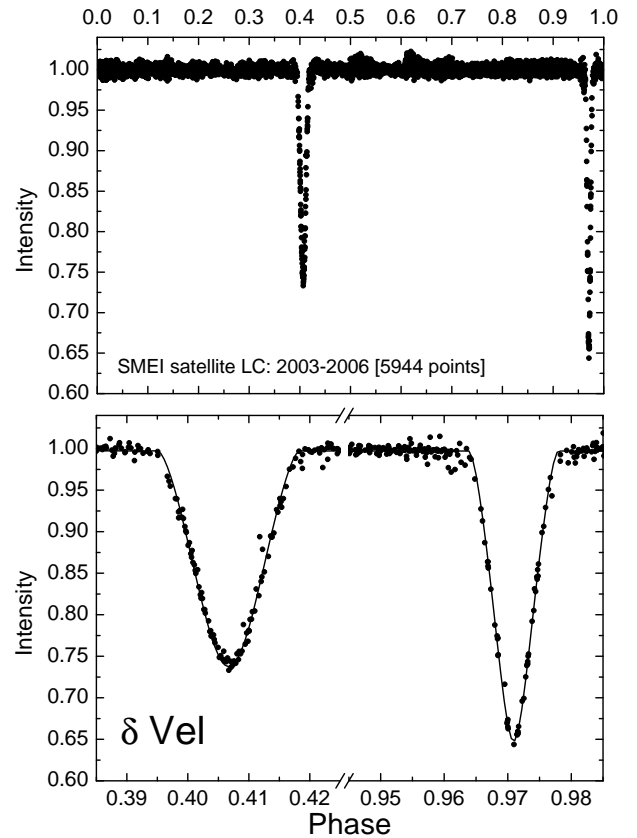


Fig. 1. Detrended and filtered (removing obvious outliers) SMEI LC of δ Vel. The data were phased using the following ephemeris for the periastron passage: $T_0 = \text{HJD } 2\,452\,528.950 + 45.15023 \times E$ (see Table 2). Only data from 2003–2006 are plotted.

The quality of the SMEI photometry has been deteriorating since the launch of the satellite. Hence, in further analysis only earlier data (2003–2006) have been used (Fig. 1).

2.2. BESO spectroscopy

Available spectroscopy of δ Velorum is very limited in spite of its brightness, $V = 1.96$. There are two high-resolution échelle spectra available in the ESO/FEROS data archive taken on November 25, 2004 and January 7, 2009 (both outside eclipses). There is practically no difference in the shape of line profiles between the two spectra nor any indication that δ Velorum is a SB2 system. The system has also been observed at ESO/HARPS. Unfortunately, spectra available in the ESO archive, do not sufficiently cover orbital cycle and are of low signal-to-noise (S/N) ratio.

New optical spectroscopy of δ Velorum has been obtained at the Cerro Armazones Observatory using the BESO échelle spectrograph fiber-fed from the Cassegrain focus of the 1.5m Hexapod Telescope (hereafter HPT, see Fuhrmann et al., 2010). Sixty-three spectra were obtained between April 2009 and April 2010. The spectra cover a 3530 – 8860Å wavelength range. The data were reduced using dedicated ESO-MIDAS scripts. The photometric reduction includes overscan, bias and flat-field correction. In the following step individual échelle orders were extracted, wavelength calibrated and normalized to the continuum. Finally, cosmic spikes have been removed. Wavelength calibration has been later improved using telluric bands close to 6900

¹ This angle transforms to longitude of periastron as $\omega = 90^\circ - \omega'$

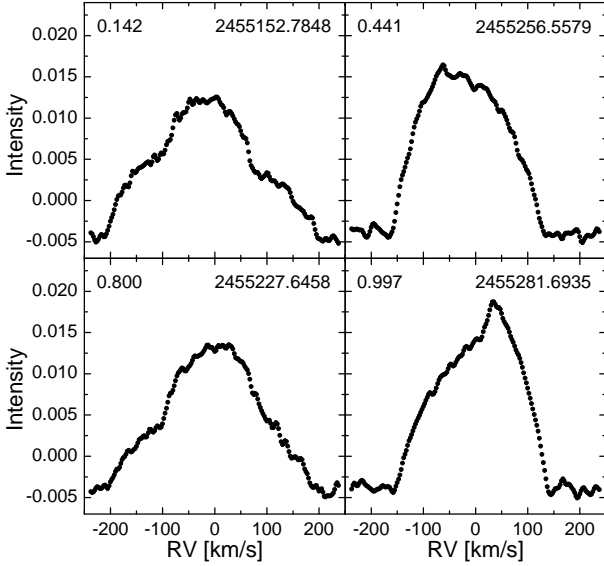


Fig. 2. Broadening functions close to the principal phases (counted from the primary eclipse, with the secondary occurring at phase 0.436): 0.142 (maximum separation of the components), 0.441 (end of the secondary eclipse), 0.800 (maximum separation of the components), 0.997 (beginning of the primary eclipse). The radial velocity system is barycentric. Full mosaic showing all BFs including best fits is available online only.

and 7600\AA using the spectrum of η CMa as the telluric template. The improved RV system is stable to about 100 m s^{-1} as indicated by the RV difference between the spectral bands mentioned above. The absolute zero point of the system has not been checked, however. Therefore the systemic velocity of δ Velorum can be offset from the true value.

According to the VLT/NACO imaging of Kervella et al. (2009) the separation of the optical pair A-B was about $0.6''$ in 2008. Because of a PSF of $3\text{--}5''$ at the HPT both visual components were included in the fiber entrance. Hence it is reasonable to assume that no light of the faint companion has got lost. The PSF required exposure times of typically 300-900 seconds, resulting in S/N ratios ranging from about 100 to 400. The journal of observations can be found in Table 1.

Sixty-three spectra more-or-less uniformly cover the orbital cycle of δ Velorum. Several spectra were intentionally taken during the eclipses. All reduced 1-dimensional spectra will be available at the CDS.

3. Data analysis

3.1. Orientation of the orbit

In principle, the orientation and eccentricity of the orbit can be estimated from the position (phase) of the secondary minimum and ratio of the minima durations (see analysis of Kellerer et al., 2007). If we denote the deeper minimum as the primary and assume that the orbit is seen edge-on, from the observed minima durations and secondary minimum phase in the case of δ Velorum one gets $e = 0.20 - 0.22$ and $\omega = 115 - 120^\circ$ (see Fig. 3). The longitude of the periastron refers to the orbit of the component eclipsed in the primary minimum. In case that we would refer to the orbit of the component eclipsed in the secondary minimum $\omega \rightarrow \omega + 180^\circ$.

The case of eccentric orbits with $i \neq 90^\circ$ is not that simple because (i) the ratio of minima depths does not reflect the ratio of

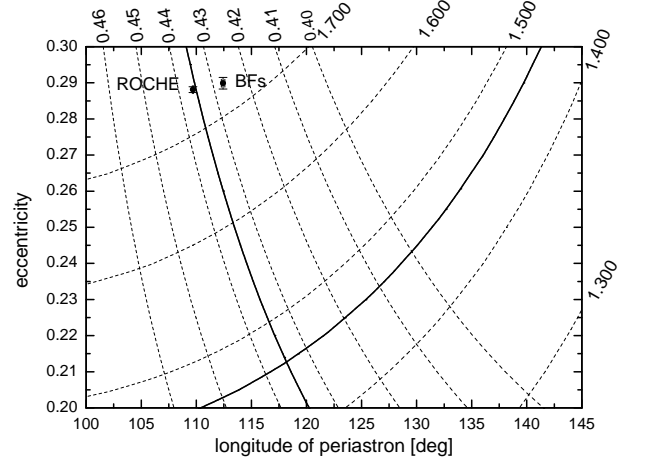


Fig. 3. Phase of the secondary minimum (labelled values are $0.40 - 0.46$; the observed phase is 0.436) and ratio of minima durations (with labelled values $1.3 - 1.7$; the observed ratio is 1.462). The lines are valid for inclination angle being $\sim 90^\circ$. Thick solid lines represent the observed values and their intersection indicates $e = 0.20 - 0.22$ and $\omega = 115 - 120^\circ$. Resulting orientation and eccentricity of the orbit plotted for simple BF modelling (Section 3.2) and ROCHE modelling (Section 3.3) shows that $i < 90^\circ$.

the surface brightness of the components (in the deeper, primary minimum even the cooler and less massive component can be eclipsed), (ii) the ratio of minima width cannot be used to find $e \sin \omega$. If $\omega \neq 90^\circ$ nor 270° , for sufficiently low inclination angle the minimum occurring further from the periastron can disappear and the observer can detect only one system of minima. This is the case of e.g., BD+37 410 (Pribulla et al., 2010) or NY Cep (see Holmgren et al., 1990).

None of the minima of δ Velorum, see Fig. 1, shows a constant brightness interval. This means that at least one minimum is partial² with $i < 90^\circ$. Hence, exact eclipse modelling is needed to arrive at reliable parameters.

3.2. Extracting Doppler information and preliminary orbit

Besides the Balmer series, there are few other strong lines in the optical spectrum of δ Velorum. The best spectral region to extract Doppler information is the blue spectrum between $4370 - 4605\text{\AA}$. In addition to the fairly strong Mg II 4481 line it contains many weaker metallic lines (mostly of Fe I) but it is devoid of hydrogen lines. This blue part of the spectra was deconvolved using a high-resolution synthetic spectrum corresponding to $T^{\text{eff}} = 9500\text{ K}$, $\log g = 4.5$, solar metallicity³ and a non-rotating star to obtain broadening functions (BFs) using the formalism originated by Rucinski (1992). Extracted BFs were smoothed, convolving with a Gaussian function ($\sigma = 10\text{ km s}^{-1}$) to match the spectral resolution of BES0.

The template provided very good match to the observed spectra indicated by the BF integral being close to unity (in average about 0.97). Using a hotter template with $T^{\text{eff}} = 10000\text{ K}$, $\log g = 4.5$ and metallicity 0.5 dex lower than the solar one resulted in BF integrals of about 1.58. The BF integral depends

² Total minimum can still be a transit, curved because of the limb darkening

³ The spectrum was taken from the Pollux database available online at <http://pollux.graal.univ-montp2.fr/>

Table 1. Journal of spectroscopic observations at Cerro Armazones Observatory. The filename contains evening date of observation encoded as yyyyymmdd. Barycentric Julian dates of mid-exposures are given. The S/N ratio was estimated from line-free continuum close to Mg II 4481 line. Phases of mid-exposures were computed using the following ephemeris for the primary minimum: $2\,447\,832.0075 + 45.15023 \times E$.

Spectrum	BJD 2 400 000+	Phase	S/N	Exp. [s]	Spectrum	BJD 2 400 000+	Phase	S/N	Exp. [s]
20090429-01.fits	54951.47364	0.6839	193	600	20100117-11.fits	55214.72408	0.5145	233	600
20091019-21.fits	55124.88346	0.5247	195	300	20100120-06.fits	55217.68788	0.5801	175	600
20091019-22.fits	55124.88728	0.5248	193	300	20100121-04.fits	55218.66777	0.6018	259	600
20091019-23.fits	55124.89110	0.5248	198	300	20100122-05.fits	55219.66618	0.6239	232	600
20091020-20.fits	55125.89151	0.5470	190	300	20100123-06.fits	55220.62644	0.6452	223	600
20091020-21.fits	55125.89535	0.5471	196	300	20100125-05.fits	55222.68527	0.6908	207	600
20091021-18.fits	55126.89139	0.5691	203	300	20100127-04.fits	55224.66181	0.7346	204	600
20091022-25.fits	55127.87589	0.5909	207	300	20100128-02.fits	55225.67460	0.7570	229	600
20091022-26.fits	55127.88004	0.5910	203	300	20100130-02.fits	55227.64583	0.8007	176	600
20091022-27.fits	55127.88384	0.5911	215	300	20100131-02.fits	55228.70596	0.8242	168	600
20091023-18.fits	55128.88626	0.6133	218	300	20100208-01.fits	55236.65951	0.0003	113	600
20091023-19.fits	55128.89015	0.6134	193	300	20100208-06.fits	55236.76622	0.0027	121	600
20091024-20.fits	55129.88268	0.6354	188	300	20100211-04.fits	55239.66155	0.0668	272	600
20091112-15.fits	55148.81797	0.0548	212	300	20100214-10.fits	55242.71579	0.1345	210	600
20091112-16.fits	55148.82182	0.0549	234	300	20100217-09.fits	55245.66592	0.1998	241	600
20091116-05.fits	55152.78108	0.1426	247	300	20100220-07.fits	55248.58518	0.2644	202	600
20091116-06.fits	55152.78487	0.1426	261	300	20100226-08.fits	55254.68385	0.3995	383	1800
20091116-09.fits	55152.85198	0.1441	221	300	20100228-04.fits	55256.55795	0.4410	262	600
20091118-04.fits	55154.76307	0.1865	213	300	20100228-13.fits	55256.72306	0.4447	281	600
20091118-05.fits	55154.76687	0.1865	224	300	20100304-07.fits	55260.66669	0.5320	293	600
20091121-07.fits	55157.77206	0.2531	222	300	20100307-10.fits	55263.64569	0.5980	296	600
20091121-08.fits	55157.77950	0.2533	234	300	20100310-09.fits	55266.63989	0.6643	221	600
20091130-02.fits	55166.79663	0.4530	153	300	20100313-06.fits	55269.63109	0.7306	215	600
20091130-03.fits	55166.80047	0.4531	160	300	20100316-08.fits	55272.61929	0.7968	328	600
20091209-08.fits	55175.70075	0.6502	100	300	20100322-07.fits	55278.62672	0.9298	265	600
20091209-09.fits	55175.70490	0.6503	100	300	20100325-07.fits	55281.60965	0.9959	276	900
20100109-09.fits	55206.71990	0.3372	193	300	20100325-10.fits	55281.69350	0.9977	287	900
20100109-10.fits	55206.72635	0.3373	205	300	20100326-06.fits	55282.57737	0.0173	333	900
20100111-12.fits	55208.76993	0.3826	163	600	20100326-10.fits	55282.68869	0.0198	314	900
20100112-09.fits	55209.75303	0.4044	158	600	20100328-09.fits	55284.60675	0.0623	400	600
20100114-07.fits	55211.69796	0.4475	167	600	20100331-06.fits	55287.57912	0.1281	274	600
20100116-07.fits	55213.69359	0.4917	251	300					

on the strength of metallic lines in the region, hence good spectra match can be provided by synthetic template of lower temperature and lower metallicity or by using a template of higher temperature and higher metallicity.

Extracted BFs clearly show that δ Velorum is a SB2. Unfortunately, profiles of the components are always blended (see Fig. 2). The orbital motion is, however, well seen from strong changes of the total width and shapes of BFs. The deformed shapes of BFs close to spectroscopic conjunctions confirm eclipses in the system. It is interesting to note that the extracted BFs do not show any presence of the visual component B in the system in spite of its expected contribution of about 3.7% (in the wide H_p passband⁴). We also produced an average spectrum of δ Velorum and extracted the corresponding BF. This way the orbital motion of the eclipsing pair is smeared-out but still no additional component could be seen. This indicates that the visual component B is also a rapid rotator or it is a SB1/SB2 system. Another possible explanation is that the spectral type of the third component is too different to be picked up in the spectrum using the A0 template.

Because the profiles of the components are never separated and we observe just blends of variable shape, it is impossible to

directly determine the RVs of the components. Hence we modelled the whole dataset (with a single set of parameters) assuming that (i) width and shape of the rotational profiles of the components do not change with phase, (ii) the relative intensity of the components is constant, (iii) limb darkening is the same for both components, (iv) there is no apsidal motion visible in our data (as indicated by the long-period of the eclipsing pair), and (v) stars rotate as solid bodies (no differential rotation). To fulfill the first two conditions, the spectra taken during the eclipses were neglected. The standard deviation of each BF has been determined from its violet part always outside of the component's profiles.

In the case of solid-body rotation and a linear limb-darkening law the rotational profile is an analytic function. The BF observed outside the eclipses is just a sum of two rotational profiles as given by Gray (1976). The limb darkening coefficient was fixed at $u_{Aa} = u_{Ab} = 0.522$ as appropriate for an A0V star ($T_A^{\text{eff}} = 9420$ K, Popper, 1980) with $\log g = 4.5$ and $\lambda = 4400$ Å. Global fitting to all observed BFs included the following parameters: orbital eccentricity e , longitude and time of the periastron passage T_0 , ω , systemic velocity V_A , sum of semi-amplitudes of the RV changes $K_{Aa} + K_{Ab}$, mass ratio $q = M_{Ab}/M_{Aa}$, background

⁴ The maximum response of the Hipparcos photometric system lies within the spectral range used to extract the BFs

Table 2. Assumed, optimized and computed parameters of the eclipsing pair in the δ Velorum system. In both cases (rotational profile fitting to BFs, Section 3.2, and full ROCHE modelling, Section 3.3) linear limb-darkening law was assumed. The orbital period, P , corresponds to the best linear fit to the Galileo and SMEI secondary minima (see Section 2.1). Coefficients of the gravity darkening, $\beta_{Aa} = \beta_{Ab}$, and bolometric albedo, $A_{Aa} = A_{Ab}$, are appropriate for radiative envelopes (see von Zeipel, 1924). Third light L_3 has been estimated for the SMEI passband using model atmospheres. For both models solid body rotation was assumed. Average temperature of the primary, T_{Aa} was fixed to correspond to observed spectral type and colors. Heliocentric Julian date of the periastron passage is given $-2452\,000$. Reduced χ_r^2 is separately given for LCs and BFs. Generalized equipotentials are given for the mean distance (not in the periastron passage). Projected rotational velocities in the case of the combined ROCHE solution were not optimized but computed from other parameters. The table lists average surface gravities and volume average radii for the components. The ratio of fluxes, I_{Ab}/I_{Aa} , is given in the SMEI passband.

	BF fitting	ROCHE
Assumed parameters		
P [days]	45.15023(7)	45.15023(7)
$\beta_{Aa} = \beta_{Ab}$	–	0.25
$A_{Aa} = A_{Ab}$	–	1.00
π [mas]	–	40.90(38)
$L_3 = L_B/(L_{Aa} + L_{Ab})$	–	0.048
T_{Aa}^{eff} [K]	–	9420
Optimized parameters		
T_0 [HJD]	529.185(11)	528.950(5)
e	0.2899(16)	0.2881(8)
i [deg]	–	89.00(3)
ω [deg]	112.43(16)	109.69(5)
Ω_{Aa}	–	34.3(4)
Ω_{Ab}	–	35.7(4)
F_{Aa}	–	43.2(7)
F_{Ab}	–	50.3(9)
$q = M_{Ab}/M_{Aa}$	0.938(11)	0.937(10)
$K_{Aa} + K_{Ab}$ [km/s]	104.8(2)	106.0(15)
V_A [km/s]	$-12.07(5)$	$-10.4(5)$
$v \sin i_{Aa}$ [km/s]	139.48(10)	139.4
$v \sin i_{Ab}$ [km/s]	146.84(13)	146.5
χ_r^2 (LC)	–	0.852
χ_r^2 (BF)	2.710	1.945
Computed parameters		
$A \sin i$ [R_\odot]	89.5(2)	90.6(9)
$M_{Aa} \sin^3 i$ [M_\odot]	2.44(2)	2.53(11)
$M_{Ab} \sin^3 i$ [M_\odot]	2.29(2)	2.37(10)
L_{Aa} [L_\odot]	–	56.3(17)
L_{Ab} [L_\odot]	–	47.1(25)
I_{Ab}/I_{Aa}	0.813(3)	0.822(4)
R_{Aa} [R_\odot]	–	2.83(4)
R_{Ab} [R_\odot]	–	2.54(5)
$\log g_{Aa}$ [cgs]	–	3.90(2)
$\log g_{Ab}$ [cgs]	–	3.97(3)

level of BFs⁵ B_0 , intensities of the profiles I_{Aa} and I_{Ab} and projected rotational velocities of the components $v_{Aa} \sin i$, $v_{Ab} \sin i$. The orbital period P was held fixed at the photometrically determined value, $P = 45.15023$ days, because of a relatively short time-span of observations.

⁵ For a perfect match of the spectral types of the template and observed star and proper rectification to the continuum it should be zero

The convergence process has been repeated starting at many (dozens) parameter sets. Modelling showed that the component eclipsed in the primary minimum is the more massive of the two.

The optimization always resulted in the same parameters (listed in Table 2) indicating uniqueness of the solution (see on-line Fig. 1 showing fits to all BFs outside eclipses). The effect of the limb darkening is small but not negligible. For the acceptable temperature range, 8750 K (A2V) to 10000 K (B9.5V), the principal parameters lie within the following ranges: $e = [0.2889, 0.2924]$, $K_{Aa} + K_{Ab} = [104.41, 105.27]$ km s⁻¹, $v_{Aa} \sin i = [139.11, 140.21]$ km s⁻¹, and $v_{Ab} \sin i = [146.48, 147.58]$ km s⁻¹. It is clear that systematic uncertainties (connected with uncertain temperature and the limb darkening coefficient) are larger than those determined from residuals and the covariance matrix. The reduced χ_r^2 corresponding to the tested temperature range changes by only 3.1% (lowest χ_r^2 occurs for $T^{\text{eff}} = 8750$ K). For any solution it is clear that the component being eclipsed in the primary minimum is the more massive of the two. The goodness of the fit, $\chi_r^2 = 2.71$ indicates underestimated errors of BFs or/and a too simple model used to fit the data.

For the solution corresponding to A0V stars, the ratio of fluxes is:

$$\frac{I_{Ab}}{I_{Aa}} = \frac{I_{Ab} v_{Ab} \sin i}{I_{Aa} v_{Aa} \sin i} = 0.813(3) \quad (1)$$

The brightness ratio should be taken with caution because in extracting BFs the same template was used for both components. In the case that the spectral type of the secondary was later (or better strength of the metallic lines was larger) the estimated light ratio is the upper estimate. Results of the following section (3.3) indicate, however, that the temperatures of the components are very similar.

The corresponding masses of the components are $M_{Aa} \sin^3 i = 2.439(20) M_\odot$, and $M_{Ab} \sin^3 i = 2.288(18) M_\odot$ (the mass ratio is then 0.938(11)). Considering the full acceptable range of temperatures, the masses fall within $2.4308 < M_{Aa} \sin^3 i < 2.4516 M_\odot$ and $2.2709 < M_{Ab} \sin^3 i < 2.2950 M_\odot$. Because the inclination angle is $\sim 89^\circ$ (see Section 3.3), the projected masses are close to the true masses (a 1% increase of masses occurs for an inclination $i = 85.3^\circ$).

The BFs, very probably, contain a weak signature of the visual component B. Its separate spectrum would, however, be needed to remove its influence on BFs and the determined orbital elements. In the case that it was a single but rapidly-rotating star (having a profile with a constant RV) it would effectively bring the components of the eclipsing pair together, reducing ($K_{Aa} + K_{Ab}$) and also affecting the derived rotational velocities. Because of severe blending of the primary and secondary lines it is also impossible to check if the components rotate as a solid body or differentially.

3.3. Simultaneous analysis of photometry and spectroscopy

Assuming that the apsidal motion is very slow⁶ and the orbital period is stable, we can combine SMEI (broadband) LC and OCA échelle spectroscopy (63 BFs) to provide consistent parameters for the system.

Modelling of the data has been performed using an updated version of the code *ROCHE* (Pribulla, 2004). The code assumes

⁶ Using formulae of Hilditch (1980), resulting parameters from Table 2 and corresponding apsidal constants adopted from Claret (2004) for 400 Myr stellar model with overshooting (see Section 4) leads to $U \sim 6$ Myr

Roche model defining the surface geometry and local gravity on the components. It is assumed (as suggested by Wilson, 1979) that the components can adjust their shape⁷ to slightly changing equipotential surfaces in the case of eccentric orbit. Generalization of the Roche model for asynchronous rotation was also applied. Surface grids are derived from icosahedron, resulting in practically equal elements. For both stars it has been assumed that the Von Zeipel (1924) law (appropriate for radiative envelopes) dictates local temperature. Single mutual reflection/irradiation has been computed.

The optimized parameters are as follows: inclination angle i , generalized equipotentials Ω_{Aa} , Ω_{Ab} , asynchronous rotation factors F_{Aa} , F_{Ab} ⁸, mass ratio q , polar temperature of the secondary T_{Ab}^{eff} , sum of semi-amplitudes $K_{Aa} + K_{Ab}$, systemic velocity V_A , longitude of periastron ω , eccentricity e , global normalization factor of BFs (should be unity in the case of perfect template match), global level of BFs background. Linear limb darkening coefficients u_{Aa} , u_{Ab} were automatically recalculated, interpolating from tables of van Hamme (1993) according to the mean surface gravity, and wavelength range (separately for LCs and BFs). Local surface intensities were interpolated from tables of Lejeune et al. (1997) for each surface grid point. Because of changing distance and shape of the components, surface grid and local parameters had to be recalculated for each step in phase (360 steps/orbit). During the eclipses a 4-times finer phase step has been used.

The scatter of *whole* individual datasets has been estimated by polynomial fitting to constant regions: in the case of the SMEI LC we used out-of-eclipse phases; for BFs parts outside the blended profile. To better restrict the solution, only eclipse parts of the SMEI LC have been used. Resulting parameters are listed in Table 2. The combined solution gives true (not projected) masses of the components as $M_{Aa} = 2.53 \pm 0.11 M_{\odot}$, $M_{Ab} = 2.37 \pm 0.10 M_{\odot}$ ($\sin^3 i = 0.99954$).

The best fits to both eclipses, as observed by the SMEI satellite, are shown in Fig. 1, fits to all BFs are available as online material only (online Fig. 2). The best fits to the BFs including eclipses do not show any systematic discrepancies. Small differences in the shapes of the minima branches of the SMEI LC can be seen, however. This can be result of simplified treatment of the limb darkening effect⁹ or small departures of the component shapes from the generalized Roche model. Comparing spectroscopic elements obtained assuming two limb-darkened rapidly rotating spheres (Section 3.2) to those obtained by the more realistic modelling assuming the Roche geometry including all proximity effects indicates good reliability of the results. The major difference is in the mass ratio and the total mass of the system (given by $K_{Aa} + K_{Ab}$), which is larger in the case of full modelling.

Because of enormous CPU time required to model deformed (and changing) shapes of the components with the orbital revolution it is practically impossible to survey the whole parameter space and possible correlations of parameters. Some properties of the solution and informational contents of the data are as follows:

- Unlike LCs, the BFs alone define eccentricity and orientation of the orbit not very well. Fixing eccentricity at different reasonable values gives acceptable range $e = [0.24, 0.33]$ without obvious correlation to ω , always being $[112, 116]^\circ$.
- The LC alone defines inclination angle very well because of small fractional radii of the components, but there is correlation between the radii of components and inclination angle. The solution shows that *both* eclipses are partial - visible surface of the component eclipsed in the minima is 35.6% (primary minimum) and 40.8% (secondary minimum).
- Including asynchronous rotation into the computation of component's shapes does not improve the solution significantly. The presence of fast asynchronous rotation would not be inferred from the photometry alone. The information content of one broad-band LC is clearly much smaller than that of many BFs obtained at different phases.
- Assuming no gravity darkening ($\beta_{Aa} = \beta_{Ab} = 0.00$) makes fits to the LCs and BFs worse by only 5% and 2% (according to χ_r^2). This means that it is impossible to reliably determine the gravity darkening coefficient from the present data.
- The combined solution shows that the secondary component is slightly hotter than the primary. This information cannot be inferred from BFs modelling alone.

4. The triple system δ Velorum

The total mass of the whole triple system δ Velorum as determined by Argyle et al. (2002) is rather uncertain: $5.71_{-1.08}^{+1.27} M_{\odot}$ (assuming the Hipparcos parallax, $\pi = 40.90 \pm 0.38$ mas). The authors give visual magnitudes of the components as $V_A = 1.97$ and $V_B = 5.55$, corresponding to the following absolute magnitudes $M_V(A) = 0.02$ and $M_V(B) = 3.60$. The visual orbit was determined based on the data from 1895 till 1999. Because of the recent periastron passage (2000.8 according to their orbit) any new positional measurements of the visual pair could significantly improve the orbit. The new observation (NACO/VLT on April 1, 2008), of Kervella et al. (2009) gives a separation of components of about $0.6''$ (their Fig. 2) and confirms the orbit of Argyle et al. (2002).

Our combined LC and BF solution gives the following luminosities for the components: $L_{Aa} = 56.3 L_{\odot}$ and $L_{Ab} = 47.1 L_{\odot}$. Taking the absolute bolometric magnitude of Sun as $M_{\odot}^{\text{bol}} = 4.75$ and bolometric correction for components of δ Vel (A0V) as B.C. = -0.15 (Popper, 1980) we get the absolute visual magnitudes of the components as $M_V(Aa) = +0.519$ and $M_V(Ab) = +0.719$. This gives a combined magnitude $M_V(A) = -0.138$, which is substantially brighter than the reliable value determined from the observed visual brightness and Hipparcos distance by Argyle et al. (2002). This simple computation, however, does not take into account the fact, that the observer faces the coldest (equatorial) part of the system. Apparent magnitudes of the eclipsing pair synthesized by the *ROCHE* code (including all proximity effects and gravity darkening), $U = 1.98 \pm 0.02$, $B = 1.94 \pm 0.02$, $V = 1.95 \pm 0.02$, $K = 1.86 \pm 0.02$ are in very good agreement with the observations: Kervella et al. (2009) found $V(Aab) = 2.00 \pm 0.02$, and $K(Aab) = 1.86 \pm 0.09$.

The positions of all three components in the H.-R. diagram together with theoretical isochrones are plotted in Fig. 4. Assuming that the third component is still on the main sequence¹⁰, its absolute visual magnitude, $M_V(B) = 3.60$, corre-

⁷ In the case of δ Velorum eccentric orbit causes just very small changes of true radii with orbital phase, e.g., $\Delta R_{\text{point}}/R \sim 7 \cdot 10^{-5}$. The shapes of components are much more affected by fast asynchronous rotation

⁸ For bound rotation, $F_{Aa} = F_{Ab} = 1$

⁹ the limb-darkening coefficients are assumed to be constant over the surface of components

¹⁰ It is least massive of the trio, with significant turn off from the Main sequence at ages higher than 1 Gyr, excluded by the evolutionary state of the eclipsing pair

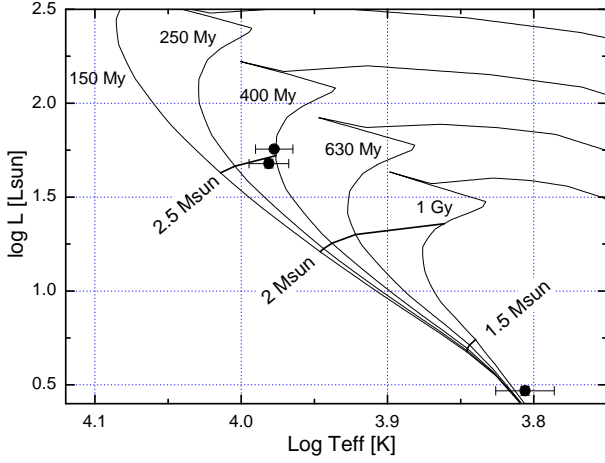


Fig. 4. Theoretical isochrones (dashed lines) for solar composition ($X = 0.70$, $Y = 0.28$, $Z = 0.02$) assuming overshooting adopted from Claret (2004). Positions of all three components of δ Velorum are shown. Thick solid lines correspond to masses $1.5 M_{\odot}$, $2 M_{\odot}$, and $2.5 M_{\odot}$. Luminosities of Aa and Ab correspond to the combined solution while for component B the luminosity was derived from the Hipparcos distance and observed visual magnitude. Horizontal error bars for the components of the eclipsing pair correspond to the surface temperature ranges due to the gravity brightening

sponds to F2-F5 spectral type or according to Cox (2000) to $T_B^{\text{eff}} = 6100 - 6700$ K and luminosity $L_B = 3.19 - 3.56 L_{\odot}$. In the H.-R. diagram component B is a bit above the Main sequence supporting the earlier limit for the spectral type, namely F2V. The positions of components of the eclipsing pair Aa, Ab plotted in Fig. 4 were derived from the combined solution to all BFs and SMEI LC for $T_{Aa}^{\text{eff}} = 9420$ K.

The observed masses and radii of components, best correspond to model predictions (Claret, 2004, $Y = 0.70$, $Z = 0.02$, and overshooting) for 400 Myr, when temperatures of components would be $T_{Aa} = 9470$ K, $T_{Ab} = 9370$ K, $R_{Aa} = 2.643 R_{\odot}$ and $R_{Ab} = 2.363 R_{\odot}$. The corresponding apsidal motion constants are $\log k_2$ (Aa) = -2.4972 and $\log k_2$ (Ab) = -2.4626 . Observed radii of stars are still about 5-6% larger, giving additional support to lower temperature and a slightly higher age - soon after 400 Myr the temperatures of components equalize (which is observed) because of the slightly faster evolution of the more massive primary component. The next isochrone available from Claret (2004) for 630 Myr predicts $T_{Aa} = 7980$ K, $T_{Ab} = 8132$ K, $R_{Aa} = 4.263 R_{\odot}$ and $R_{Ab} = 3.393 R_{\odot}$. The evolution of the components could, however, be affected by fast rotation, making the main-sequence phase last longer (see e.g., de Mink, 2010).

5. Discussion and future work

Our new data has enabled the first sound analysis of the eclipsing pair Aab in the δ Velorum system. The main results are as follows:

- Both minima are partial. For the given orientation of the orbit and (fairly similar) radii of components total eclipse and annular transit occur only if $i > 89.8^{\circ}$.
- The components of the eclipsing pair are factor 2 smaller than derived interferometrically by Kellerer et al. (2007).

- The brightness ratio of brightness of components in the SMEI passband (close to the R passband) is about 0.823. The components are of similar temperature, however, both very probably of spectral type A1V. This is strongly supported by good accord of the synthetic depth of the primary minimum in the K passband $\Delta\text{mag } I = 0.430$, while Kervella et al. (2009) determined $\Delta\text{mag } I = 0.440 \pm 0.011$ from the NACO imaging during the primary eclipse.
- There is no apsidal motion in the system observed during the 6-year time-series of the SMEI data as indicated by the observed times of the minima.
- Photocenter motion of the eclipsing pair (corresponding to our solution) is only about 1 mas: it was not detected by the Hipparcos satellite.
- Both components rotate very fast: the primary at about 56% of the break-up velocity, the secondary at about 62%. This also means that the components are strongly deformed. In the case that the surface fully follows generalized ROCHE model, the polar flattening of the components is 1/10 and 1/12. Because of the fast rotation surface temperatures are rather non-uniform. Von Zeipel theorem predicts the following ranges: $9220 \text{ K} < T_{Aa}^{\text{eff}} < 9780 \text{ K}$ and $9280 \text{ K} < T_{Ab}^{\text{eff}} < 9880 \text{ K}$ ¹¹. This effect should be confirmed by long-baseline interferometry.
- The best fits to the BFs extracted during the primary transit (spectra taken at phases 0.995, 0.997, 0.000, and 0.002) shows just slight deviations indicating that the rotational axis of the primary component is close to being perpendicular to the orbital plane. The secondary minimum, occurring around phase 0.436, is not sufficiently covered (a single spectrum at phase 0.441) by the spectroscopic observations to get any clue of the rotational axis orientation.
- The spectral type of δ Velorum A is most probably A1V, although different approaches lead to a fairly wide range of results: (i) BF strength indicates $T_A^{\text{eff}} = 9500$ K (A0V); see Section 3.2 (ii) combination of observed visual brightness, Hipparcos distance, and radii of the components (simultaneous solution in Section 3.3) supports a similar temperature, 9420 K, (iii) observed colors $U - V = 0.11$, $B - V = 0.04$, $V - R = 0.05$, $V - I = 0.09$ indicates a later classification, A1-2V (see Stickland & Hucht, 1977), (iv) shape and intensity of the H_{β} line (in our BESO spectra) best corresponds to a higher temperature, $T_A^{\text{eff}} = 10000$ K and $\log g_A = 4.5-4.6$ (B9.5V) (v) Gray (2006) gives a spectral type of A1Va(n), $T^{\text{eff}} = 9021$ K, $\log g = 3.79$, $\log [M/H] = -0.33$. Because the system is very close, no interstellar reddening is expected. On the other hand, the presence of circumstellar material around δ Velorum cannot be fully excluded.

In spite of significant progress, the astrophysical parameters of δ Vel should still be verified. The total mass of the system is slightly affected by the unknown nature (multiplicity, rotation rate) of the third component (δ Velorum B). To correctly remove its contribution to the observed line profiles it is necessary to take its spectrum separately. This task will not be easy: the separation between the components will be getting smaller until 2013 when it reaches $0.38''$. Then the separation would slowly increase until 2067, reaching about $2.9''$.

Our phase-resolved spectra could still be subject to the Fourier disentangling (see Hadrava, 1995) to obtain separate spectra of components and their astrophysical parameters ($\log g$,

¹¹ Surface temperature is increasing from the equator to the poles

T^{eff} , metallicity etc.). Because of fast rotational mixing, any chemical peculiarity is, however, excluded.

Most important would be the combination of the present data with long-baseline interferometry which could possibly detect flattening of the components and "polar caps" brightening resulting from the fast rotation. This additional dataset would break parameter correlations complicating present modelling.

Additional high-resolution spectroscopy should be secured during the eclipses to study Rossiter-McLaughlin effect. Photometric eclipse modelling can still be improved by dedicated multi-color photometry of the transits, important for better definition of the surface brightness ratio.

Another possibility to further improve the outer visual orbit is to use timing of the minima of the eclipsing pair which should show light-time effect. Expected semi-amplitude, for the visual orbit of Argyle et al. (2002), is about 1.5 hour. In the view of large $v \sin i$ of the components and blending of their profiles, systemic-velocity changes of the eclipsing would hardly be detectable and useful.

Acknowledgements. M.V. and T.P. acknowledge support from the EU in the FP6 MC ToK project MTKD-CT-2006-042514. This work has partially been supported by VEGA project 2/0038/10.

This publication is supported as a project of the Nordrhein-Westfälische Akademie der Wissenschaften und der Künste in the framework of the academy program by the Federal Republic of Germany and the state Nordrhein-Westfalen.

M.A. acknowledges research funding granted by the *Deutsche Forschungsgemeinschaft* (DFG) under the project RE 1664/4-1. A.B. acknowledges support from DFG in program NE 515/32-1.

The research made use of the SIMBAD database, operated at the CDS, Strasbourg, France.

References

- Argyle, R.W., Alzner, A., & Horch, E.P. 2002, *A&A*, 384, 171
 Bruntt, H., Southworth, J., Torres, G., Penny, A.J., Clausen, J.V., Buzasi, D.L. 2006, *A&A*, 456, 651
 Claret, A., 2004, *A&A*, 424, 919
 Cox, C.W. 2000, *Allens Astrophysical Quantities* (Springer Verlag)
 de Mink, S. 2010, PhD thesis, Utrecht University
 European Space Agency 1997, *The Hipparcos and Tycho Catalogues* (ESA SP-1200)(Noordwijk: ESA)
 Fuhrmann, K., Chini, R., Hoffmeister, V.H., Lemke, R., Murphy, M., Seifert, W., Stahl, O. 2010, *MNRAS*, in press
 Gáspár, A., Su, K.Y.L., Rieke, G.H., Balog, Z., Kamp, I., Martínez-Galarza, J.R., Stapelfeldt, K. 2008, *ApJ*, 672, 974
 Goss, K.J.F., Karoff, C., Chaplin, W.J., Elsworth, Y., Stevens, I.R. 2010, *MNRAS*, (in press)
 Gray, F.D., 1976, *The Observation and Analysis of Stellar Photospheres* (New York: Wiley)
 Gray, R.O., Corbally, C.J., Garrison, R.F., McFadden, M.T., Bubar, E.J., McGahee, C.E., O'Donoghue, A.A., Knox, E.R. 2006, *AJ*, 132, 161
 Hadrava, P. 1995, *A&AS*, 114, 393
 Hilditch, R.W., 2001, *An Introduction to Close Binary Stars*, (Cambridge University Press), p. 140
 Holmgren, D.E., Hill, G., Fisher, W., Scarfe, C.D. 1990, *A&A*, 231, 89
 Kellerer, A., Petr-Gotzens, M.G., Kervella, P. & Coudé du Foresto, V. 2007, *A&A*, 469, 633
 Kervella, P., Thévenin, F., Petr-Gotzens, M.G. 2009, *A&A* 493, 107
 Lejeune, Th., Cuisinier, F., Buser, R. 1997, *A&AS* 125, 229
 Levato, O.H. 1972, *PASP*, 84, 584
 Otero, S.A., Fieseler, P.D., Lloyd, C. 2000, *IBVS* No. 4999
 Popper, D.M. 1980, *ARA&A*, 18, 115
 Pribulla, T. 2004, in *Spectroscopically and Spatially Resolving the Components of the Close Binary Stars*, (eds.) R.W. Hilditch, H. Hensberge & K. Pavlovski, *ASP Conference Series*, Vol. 318, p117
 Pribulla, T., Rucinski, S.M., Latham, D.W., Quinn, S.N., Siwak, M., Matthews, J.M., Kuschnig, R., Rowe, J.F., Guenther, D.B., Moffat, A.F.J., Sasselov, D., Walker, G.A.H., Weiss, W.W. 2010, *AN*, 331, 397
 Royer, F., Gerbaldi, M., Faraggiana, R., Gómez, A.E. 2002, *A&A*, 381, 105
 Rucinski, S.M. 1992, *AJ*, 104, 1968
 Sreckley, S.A., Stevens, I.R. 2008, *MNRAS*, 388, 1239
 Stickland, D.J., van der Hucht, K.A. 1977, *A&A*, 54, 883
 Tarrant, N.J., Chaplin, W.J., Elsworth, Y.P., Sreckley, S.A., Stevens, I.R. 2008, *A&A*, 492, 167
 van Hamme, W. 1993, *AJ* 106, 2096
 von Zeipel, H. 1924, *MNRAS*, 84, 665
 Walker, G., Matthews, J., Kuschnig, R., Johnson, R., Rucinski, S.M., Pazder, J., Burley, G., Walker, A., Skaret, K., Zee, R., Grocott, S., Carroll, K., Sinclair, P., Sturgeon, D., Harron, J. 2003, *PASP*, 115, 1023
 Wilson, R.E. 1979, *ApJ*, 234, 1054

